American Mineralogist, Volume 81, pages 418–428, 1996

Single-crystal IR spectroscopy of pyrope-almandine garnets with minor amounts of Mn and Ca

A.M. HOFMEISTER,[1] T.J. FAGAN,[2] K.M. CAMPBELL,[2] AND R.B. SCHAAL[2]

[1]Department of Earth and Planetary Sciences, Washington University, St. Louis, Missouri 63131, U.S.A.
[2]Department of Geology, University of California, Davis, California 95616, U.S.A.

ABSTRACT

Mg^{2+}-Fe^{2+} substitution in the dodecahedral interstice of eight natural single crystals and two synthetic polycrystalline garnets was investigated by measurement of mid- and far-infrared (IR) reflectance spectra across the pyrope-almandine [Py-Al = $(Mg_x$-$Fe_{1-x})_3Al_2Si_3O_{12}$] binary. The effect of minor Mn and Ca substitution was investigated by comparison with spectra of four additional natural garnets, $Py_8Al_{82}Sp_{10}$ and $Py_{10}Al_{76}Sp_{14}$, where Sp denotes spessartine ($Mn_3Al_2Si_3O_{12}$), and $Py_{72}Al_{18}Gr_{10}$ and $Py_{54}Al_{36}Gr_{10}$, where Gr denotes grossular ($Ca_3Al_2Si_3O_{12}$). Data obtained from the two synthetic polycrystals are in excellent agreement with data from the single crystals. Frequencies of all 17 IR-active fundamental modes were observed in all specimens except pyrope. Of the 17 modes, 16 show linear correlations between frequency and composition along the pyrope-almandine join. The remaining mode, assigned to translations of the divalent cations against the O framework, exhibits two-mode behavior. The trends show that two modes in pyrope are accidentally degenerate. Frequencies of garnets with up to 10 mol% spessartine and grossular contents lie on the trends defined by the pyrope-almandine samples with negligible impurities. However, one to three additional modes are seen for some intermediate compositions, apparently resulting from either resonances among combination modes or two-mode behavior due to high Ca contents. The nearly linear behavior of the modes indicates that mixing should be close to ideal for the pyrope-almandine series because the lattice contribution dominates heat capacity, entropy, and compressibility.

INTRODUCTION

This article is one in a series using infrared (IR) spectroscopy to probe the various chemical substitutions and solid solutions possible in garnet (Hofmeister and Chopelas 1991; Hofmeister and Campbell 1992; Lu et al. 1993; McAloon and Hofmeister 1993). As discussed by McAloon and Hofmeister (1995), spectroscopic studies of solid solutions are motivated by (1) the observation that macroscopic properties vary nonlinearly with some compositional series, (2) the existence of models that allow for the calculation of macroscopic properties from microscopic behavior, and (3) the insight provided by IR vibrations into the nature of the chemical bond. The pyrope-almandine $(Mg_xFe_{1-x})_3Al_2Si_3O_{12}$ binary is of interest because of the ubiquitous occurrence of such garnets and because the Mg-Fe^{2+} exchange is exceedingly common in minerals. This study provides the ground work for further investigation into the interesting behavior of the more complex chemical compositions found in aluminous garnets.

Previous IR spectra of the pyrope-almandine (Py-Al) binary were obtained from KBr dispersions of synthetic polycrystals and are limited to peak positions above 400 cm^{-1} (Geiger et al. 1989). This study presents complete IR reflectance data for 12 natural and two synthetic samples that lie close to or on the pyrope-almandine binary. Two natural samples bearing spessartine (Sp), $Mn_3Al_2Si_3O_{12}$, and two natural samples bearing grossular (Gr), $Ca_3Al_2Si_3O_{12}$, are included to assess the effect of minor deviations from the binary compositions. Natural samples were primarily used, despite slight uncertainties in site occupancy, because single crystals yield complete and quantitative IR measurements (e.g., Wooten 1972; Hofmeister 1995). It is not necessary to obtain absorption spectra because these data can be extracted from reflectance spectra (e.g., Wooten 1972). We find that frequencies of the 17 IR-active vibrations in pyrope-almandine with <10 mol% spessartine or grossular depend approximately linearly on composition. This relationship is consistent with ideal mixing.

EXPERIMENTAL METHODS

Chemical analyses were obtained with a Cameca SX-50 Electron Microprobe using standard microprobe techniques. Operating conditions for samples 3, 7, 9, 11, and 17 consisted of a 15 keV acceleration voltage, 20 nA sample current, and 40 s counting times. For the other samples, 10 nA current and 10 s counting times were used. Natural minerals were used as standards. Chemical zonation was not observed. Published compositions were

0003–004X/96/0304–0418$05.00

TABLE 1. Sample descriptions

Index	Approx. comp.	Source	Sample	Locality	Reference
3*	$Py_{95}Al_5$	R.M. Hazen, J.R. Smyth	SDM-1	Dora Maria Massif, Italy	Chopin (1984)
18**†	$Py_{72}Al_{28}$	UCD museum	R-8a	Roberts Victor Kimberlite, S. Africa	MacGregor and Manton (1986)
9‡	$Py_{67}Al_{33}$	R.B. Schaal	MOS-4x	Moses Rock Dike, UT	Schaal (1991)
7‡	$Py_{60}Al_{40}$	R.B. Schaal	MOS-2x	Moses Rock Dike, UT	Schaal (1991)
40	$Py_{58}Al_{42}$	UCD museum	UCD SM 1597	Macon Co., NC	Deer et al. (1982) p. 503
43§	$Py_{54}Al_{46}$	A. Koziol	AK 51	synthetic polycrystal	Koziol and Newton (1989)
20**	$Py_{54}Al_{46}$	UCD museum	R-71a	Roberts Victor Kimberlite, S. Africa	MacGregor and Manton (1986)
33	$Py_{44}Al_{56}$	F. Barker		De Luca Pit, Cortlandt, NY	Barker (1964)
34	$Py_{40}Al_{60}$	F. Barker		Emery Hill, Cortlandt, NY	Barker (1964)
11	$Py_{18}Al_{82}$	R.M. Hazen, J.R. Smyth	NMNH 107105	Emerald Creek, Latah Co., ID	Novak and Gibbs (1971), Hietanen (1963)
38	Py_6Al_{94}	W.C. Metropolis	Harvard 102872	Harney Peak District, SD	
41	Py_0Al_{100}	S.R. Bohlen	UCD probe std.	synthetic polycrystal	
30	$Py_8Al_{82}Sp_{10}$	T.J. Fagan		Mt. Monadnock, NH	Thompson (1985)
17	$Py_{10}Al_{76}Sp_{14}$	UCD museum	SM 1090	Fort Wrangle, AK	Pabst (1943)

* Similar samples from this locality have OH^- in concentrations of 0.002–0.003 wt% H_2O (Rossman et al. 1989).

** These two samples have high Ca (10 mol% grandite): MacGregor and Manton (1986).

† Samples with similar chemistry from the Monestary Mine kimberlite in South Africa have OH^- in concentrations of 0.0056 wt% H_2O (Bell et al. 1995).

‡ These two samples have OH^- in concentrations of 0.11 wt% H_2O (Schaal et al., in preparation).

§ This polycrystalline sample is 53.9 mol% pyrope, 41.4 mol% almandine, and 4.7 mol% grossular (Koziol and Newton 1989).

used for samples 18 and 20 (MacGregor and Manton 1986) and 43 (Koziol and Newton 1989).

Infrared reflectance spectra were obtained at ambient temperature and at resolutions of 1.0 or 2.0 cm^{-1} using an evacuated Bomem DA3.02 Fourier-Transform Interferometer (FTIR). The spectrometer is equipped with a mercury cadmium telluride detector and KBr beamsplitter for the range of 450–4000 cm^{-1} and with a silicon bolometer and Mylar beamsplitters (3, 6, or 12 μm) for wavelengths below 600 cm^{-1}. Spectra were collected using a Spectatech FTIR microscope from samples of 1–12 mm diameter with random crystal orientation that were polished on one side. For the synthetic samples, plates of polished polycrystals were used. A Kramers-Kronig analysis (e.g., Andermann et al. 1965) was performed on merged reflectance spectra [see Hofmeister and Chopelas (1991) for procedural details]. Longitudinal optic (LO) peak positions were obtained from minima in the imaginary part of the dielectric function $\mathrm{im}[1/(\epsilon_1 + i\epsilon_2)]$, and transverse optic (TO) peak positions were obtained from maxima in the dielectric function ϵ_2. Uncertainties in peak positions of ± 1–0.01 cm^{-1} are related to peak widths because the accuracy of the FTIR spectrometer is an order of magnitude smaller. Absorptivity was calculated from $\alpha(\nu) = 2\pi\nu\epsilon_2(\nu)/n(\nu)$, where α is absorptivity, n is the index of refraction (calculated from the reflectivity, see, e.g., Wooten 1972), and ν is frequency.

CHEMICAL COMPOSITION AND SAMPLE DESCRIPTION

To examine IR spectra of garnets in the pyrope-almandine-grossular ternary, 43 natural single crystals and two synthetic compositions were obtained from the individuals listed in Table 1 and in the Acknowledgments or from the University of California, Davis, collection. Physical and chemical properties of all 43 samples collected are described by Schaal et al. (in preparation). Virtually all samples have weak (0.0001–0.0006) and undulatory birefringence. This property is intrinsic as it is observed in unpolished crystal fragments. Samples that appeared isotropic were either too thin or too fine grained to observe weak anisotropy. Schaal et al. (in preparation) propose that the anomalous optical properties originate in strain.

Ten samples with <10 mol% total spessartine, grossular, andradite ($Ca_3Fe_2Si_3O_{12}$), and uvarovite ($Ca_3Cr_2Si_3O_{12}$) components (Table 1) approximate the pyrope-almandine binary. Their average chemical analyses are reported (Table 2). Individual microprobe analyses may be obtained from the authors. Spessartine and calcic garnet contents were added to the almandine contents of Table 2 to describe the approximate position along the pyrope-almandine join (Table 1). This approximation is reasonable because Mg in pyrope is considerably lighter and smaller than any of the other cations but is tested by comparing the Mn- and Ca-rich samples to those with similar $Mg/(Mg + Fe^{2+})$ ratio and by representing the binary by alternate approaches.

Two garnets with slightly more Ca (samples 18 and 20 in Table 2) are included for comparison. Two additional spessartine-bearing samples (17 and 30) were studied to investigate the effect of Mn. A manuscript on the IR spectra of samples with higher amounts of Ca is forthcoming (Hofmeister et al. in preparation).

Most samples have low amounts of TiO_2 (<0.04 wt%) except for sample 18, which has 0.18 wt% TiO_2, and samples 33 and 34, which have roughly 0.3 wt% TiO_2. Cr contents are also low (<0.06 wt%) except for samples 7 and 18, which have, respectively, 0.15 and 0.25 wt% Cr_2O_3 (Table 2). It is likely that a significant proportion of the

TABLE 2. Average microprobe analyses

Sample	3	18*	9	7	40	43**
			Weight percent†			
SiO_2	43.44(26)	42.56	41.44(26)	40.46(22)	39.93(12)	41.06(46)
TiO_2	0.03(1)	0.18	0.03(2)	0.04(2)	0.010(5)	0.02(3)
Al_2O_3	25.43(10)	21.75	24.00(16)	23.60(7)	23.23(5)	23.20(28)
Cr_2O_3	0.01(1)	0.25	0.06(2)	0.15(5)	0.02(2)	0.02(2)
MgO	27.63(7)	20.86	19.04(25)	16.81(15)	15.88(13)	14.84(80)
CaO	0.76(3)	3.81	2.92(3)	2.89(7)	1.13(3)	1.70(57)
MnO	0.02(1)	0.29	0.19(2)	0.33(3)	0.90(8)	0.02(4)
FeO	1.85(3)	9.00	12.64(20)	16.41(20)	18.46(8)	19.67(90)
Fe_2O_3‡		1.19‡				
Total	99.17	99.89	100.32	100.69	99.57	100.54
Points sampled	7	n.r.	6	8	4	8
			Cations			
Si	5.942	6.064	5.932	5.884	5.914	6.024
Ti	0.004	0.020	0.004	0.004	0.002	0.003
Al	4.100	3.654	4.048	4.044	4.056	4.010
Cr	0.000	0.028	0.008	0.018	0.002	0.003
Mg	5.742	4.432	4.060	3.644	3.506	3.244
Ca	0.110	0.582	0.448	0.450	0.180	0.268
Mn	0.000	0.036	0.022	0.042	0.112	0.003
Fe^{2+}	0.212	1.072	1.510	1.963	2.288	2.413
Fe^{3+}_{oct}‡		0.128				
Fe^{3+}_{tet}§				0.033		
			Components‖			
Uv	0.0	0.7	0.2	0.5	0.1	0.1
An	0.0	3.4‡	0.0	0.0	0.0	0.0
Gr	1.8	5.4	7.2	7.0	2.9	4.4
Py	94.6	72.4	67.2	60.0	57.6	54.7
Sp	0.00	0.6	0.4	0.7	1.8	0.1
Al	3.6	17.5	25.0	31.8	37.6	40.7

* MacGregor and Manton (1986).

** Koziol and Newton (1989) reported 53.9 mol% pyrope, 41.4 mol% almandine, and 4.7 mol% grossular.

† The mean and standard deviation are reported.

‡ Because the Al content was not sufficient to fill the octahedral site, a portion of Fe was concluded to be Fe^{3+} (MacGregor and Manton 1986).

§ For these samples, a small amount of Fe was allocated to the tetrahedral site because the dodecahedral site was overfilled and the tetrahedral site was underfilled.

‖ In the recalculation, all Fe was assumed to be Fe^{2+} (unless indicated), and the Ti and the Al in excess of 2 (or 4) were assumed to be tetrahedrally coordinated, unless indicated.

The Ti is assumed to be octahedrally coordinated and is included with the andradite component.

samples lack Ti and Cr. The low amounts detected (~0.02 wt%) appear to be a blank because this magnitude was observed in the analysis of the synthetic sample 43, which lacked these elements.

Octahedrally coordinated Fe^{3+} is unlikely to be present in all the binary samples except 33 because the amount of Al present is sufficient to fill the octahedral site. Moreover, Fe^{3+} could be tetrahedrally coordinated (e.g., Dowty 1971; Deer et al. 1982; Huggins et al. 1977a, 1977b; Schwartz et al. 1980) because the small amount of Fe in excess of the cation proportions expected for the dodecahedral site (Table 2) is comparable to the small Si deficiencies observed. In contrast, it is possible that ternary, Ca-rich samples 18 and 20 have significant andradite components (about 4 mol%) because the measured concentrations of Al and Cr do not fill the octahedral site (McGregor and Manton 1986). Similarly, sample 33 may have 1.33 mol% andradite.

Trace amounts of H have been detected in samples from the same localities. The study of Rossman et al. (1989) suggests that sample 3 should have ~0.003 wt% H_2O. Work in preparation from this laboratory shows that samples 7 and 9 each have 0.11 wt% H_2O incorporated as OH^-. This amount agrees well with H_2O contents published for chemically similar garnets (Aines and Rossman 1984a, 1984b). For all samples, absorbance spectra that were calculated from the reflectance showed no evidence of hydrous impurities, suggesting that the H_2O contents are <0.4 wt% (McAloon and Hofmeister 1995). Such low values are consistent with previous data on pyrope-almandine (Aines and Rossman 1984a, 1984b; Rossman et al. 1989; Bell et al. 1995).

The above uncertainties in site occupancy and the effect of impurities on our spectral data are considered in the Discussion and Conclusions section.

RESULTS

IR reflectance spectra

All 14 garnets examined have intensity patterns (Fig. 1) that are characteristic of IR reflectance spectra for silicate garnets (cf. Hofmeister and Chopelas 1991). All 17

TABLE 2.—*Continued*

20*	33	34	11	38	30	17
			Weight percent†			
41.03	39.86(26)	37.3(4)	36.94(16)	35.32(29)	36.22(18)	35.96(4)
0.21	0.26(20)	0.16(5)	0.020(8)	0.04(4)	0.00	0.02(2)
21.31	22.44(16)	21.9(2)	21.68(5)	21.06(20)	21.26(17)	20.87(2)
0.13	0.03(1)	0.03(3)	0.01(1)	0.02(3)	0.00	0.02(1)
3.65	11.88(20)	10.6(2)	4.74(9)	1.48(17)	2.10(3)	2.55(5)
14.36	2.42(7)	2.6(1)	1.31(3)	2.23(21)	0.76(2)	0.92(5)
1.22	1.00(6)	1.5(1)	0.020(5)	0.78(41)	36.90(7)	6.40(52)
16.35	23.41(44)	24.6(4)	36.56(20)	39.27(65)	4.49(20)	32.66(68)
1.56‡						
99.82	101.45	98.7	101.28	100.20	101.73	99.39
n.r.	16	47	5	51	3	5
			Cations			
6.090	5.963	5.809	5.860	5.803	5.850	5.896
0.024	0.014	0.019	0.002	0.005	0.00	0.002
3.728	3.943	4.028	4.052	4.079	4.047	4.034
0.016	0.004	0.004	0.000	0.003	0.00	0.004
3.176	2.648	2.461	1.120	0.362	0.504	0.622
0.580	0.389	0.436	0.222	0.392	0.132	0.162
0.052	0.126	0.196	0.004	0.109	0.614	0.890
2.030	2.837	3.062	4.810	5.297	4.843	4.476
0.174	0.053					
	0.018	0.14	0.04	0.10	0.14	
			Components‖			
0.4	0.1	0.1	0.0	0.1	0.0	0.1
5.0‡#	1.3‡	0.0	0.0	0.0	0.0	0.0
4.5	5.0	7.0	3.6	5.8	2.2	2.5
54.4	43.9	40.0	18.3	6.4	8.3	10.1
0.9	2.1	3.2	0.1	1.7	10.1	14.5
34.8	47.6	49.7	78.0	86.0	79.4	72.8

IR bands expected from symmetry analysis were observed in samples with almandine contents >40 mol%, whereas 14 obvious modes and two weak bands (near 650 and ~100 cm^{-1}) were seen in end-member pyrope. One to three extra modes were seen in some intermediate compositions (Fig. 1). Peaks are labeled according to the nomenclature of Tarte (1965) and Moore et al. (1971). Band assignments are discussed below.

The signal-to-noise ratio of the reflectance spectra is high (Fig. 1). The small amount of noise present near 100 cm^{-1} in some spectra is due to low absolute transmission near the spectral limits of the detector and beamsplitter.

The spectra of the two polycrystalline synthetics, samples 43 and 41, do not noticeably differ from the spectra of the natural single crystals (Fig. 1). Band widths and frequencies are nearly the same, and the intensity profiles are markedly similar. No extra features were observed.

The dielectric functions obtained by Kramers-Kronig analysis (Fig. 2) are well behaved (see, e.g., the ideal cases presented by Wooten 1972), except for sample 20, and are similar to those measured previously for garnets. The incorrect negative values of ϵ_2 for sample 20 are probably due to a poorly resolved doublet occurring near 445 cm^{-1}. For this sample, the TO positions (Table 3) were estimated from the reflectivity data. Dielectric functions of samples 18, 7, 40, 43, and 33 are not shown because these are similar to samples 3, 9, 9, 20 [im/(1/ϵ)], and 34, respectively. Samples 11, 38, and 30 are not shown because the dielectric functions of samples 11, 38, 41, 17, and 30 are all similar.[1]

Many samples, including the end-members, display a weak peak near 750 cm^{-1} (Table 3). This feature is common in garnet spectra (Moore et al. 1971; Hofmeister and Chopelas 1991; McAloon and Hofmeister 1993) and is likely an overtone because combinations of lower frequency fundamentals in the affected samples can be found that sum to comparable frequencies. In sample 3, for example, possible combinations allowed by symmetry are 422 + 336 = 758 cm^{-1}, 2 × 383 = 766 cm^{-1}, and 535 + 220 = 755 cm^{-1}; similar combinations hold for the other samples.

An extra feature between 500 and 510 cm^{-1} is observed in all intermediates with pyrope content between 18 and 68 mol% and in one of the spessartine-rich samples (Table 3). This peak also appears to be an overtone; possible combinations are 341 + 157 = 498 cm^{-1} and 378 + 123 = 501 cm^{-1} for sample 40, for example.

For samples 18 and 20, additional weak peaks occur at 815, 292, and 178 cm^{-1}. The 292 and 178 cm^{-1} peaks clearly arise from the high Ca contents of sample 20

[1] A copy of Fig. 2 in its entirety may be obtained from the authors upon request. It may also be ordered as Document AM-96-608 from the Business Office, Mineralogical Society of America, 1015 Eighteenth Street NW, Suite 601, Washington, DC 20036, U.S.A. Please remit $5.00 in advance for the microfiche.

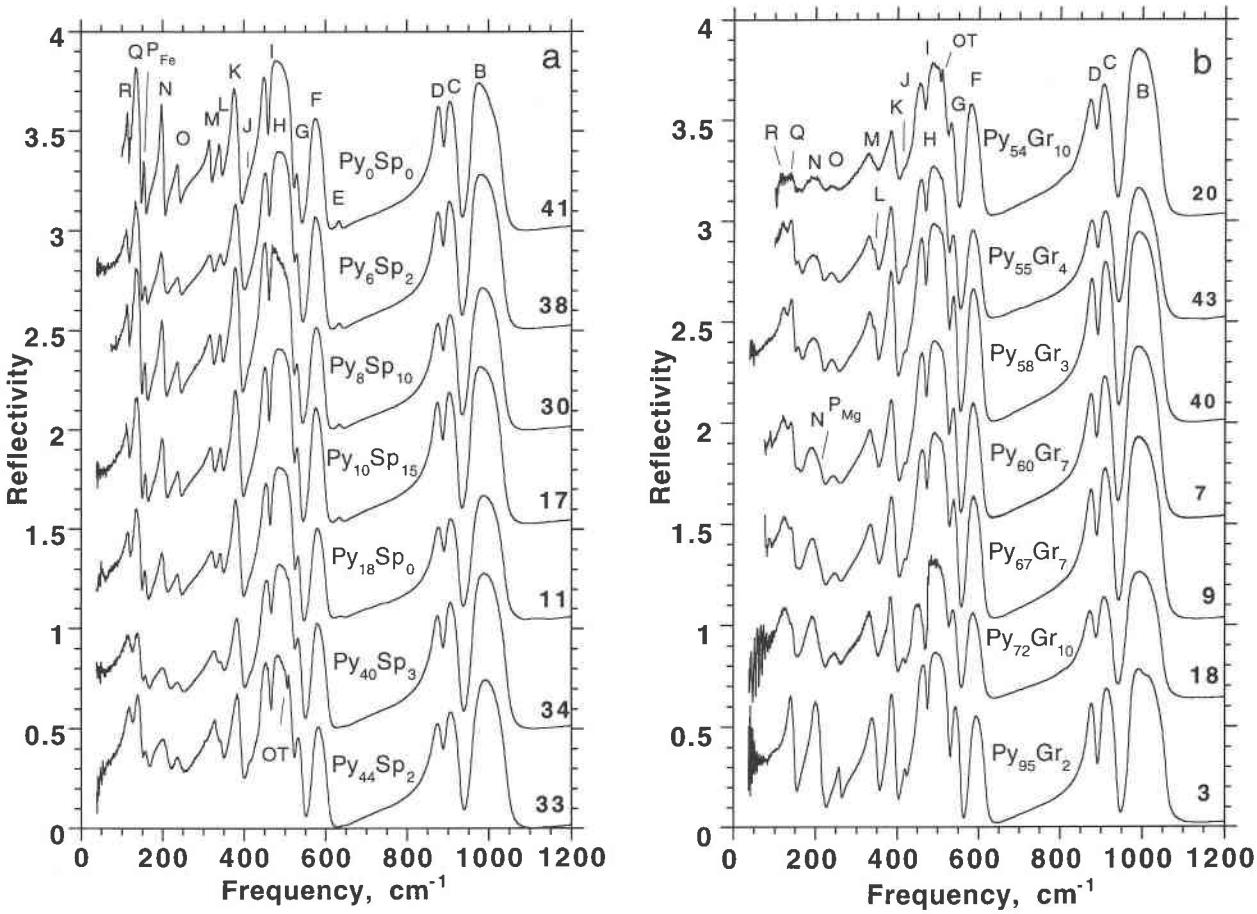

FIGURE 1. Single-crystal reflectance spectra for almandine-rich (**a**) and pyrope-rich (**b**) garnets. Pyrope (Py) content is given for each sample (middle). Spessartine (Sp) contents are shown for the almandine-rich samples [which generally have low grossular (Gr) content], and grossular contents are shown for the pyrope-rich samples (which have low spessartine content). Sample number is on the right. Noise or interference fringes are present in some spectra below 100 cm^{-1}. Peaks are labeled with the nomenclature of Tarte (1965) and Moore et al. (1971).

(grossular + andradite + uvarovite contents equal 10 mol%) in that these peak positions are near those of pure grossular (McAloon and Hofmeister 1993) and equal those observed for ternary grossular-pyrope-almandine garnets (Hofmeister et al. in preparation). Peaks in sample 18 are too broad to resolve extra bands at these positions. The 292 and 178 cm^{-1} peaks result from two-mode behavior (e.g., Chang and Mitra 1968; see also the Discussion and Conclusions section). The band near 815 cm^{-1} appears to be an overtone originating from a different series of combinations, e.g., 574 + 250 = 824 cm^{-1}, 417 + 417 = 834 cm^{-1}, 476 + 328 = 804 cm^{-1}, and 445 + 381 = 826 cm^{-1} for sample 18.

Compositional dependence of IR modes

The intensity pattern of the series gradually changes from that of pyrope to almandine (Figs. 1 and 2). The intensity of the mode at 220 cm^{-1} in pyrope decreases in the intermediates as their almandine content increases, disappearing near the middle of the binary. Another mode at 158 cm^{-1} in almandine cannot be traced completely across the binary.

Most peak positions (Table 3) increase with pyrope content. Least-squares analyses indicate that TO-mode frequencies depend linearly on mole-percent pyrope (Fig. 3a). Thus, frequency depends linearly on Mg or Fe content or on the Mg/(Mg + Fe^{2+}) ratio. The slopes range from −0.06 to 0.31 cm^{-1}/mol% pyrope, but most lie near 0.1 cm^{-1}/mol% pyrope (Table 4). Two pairs of peaks coalesce in the very pyrope-rich garnet, indicating that the 134 and 336 cm^{-1} peaks in pyrope are both accidentally degenerate. The two peaks that cannot be traced completely across the series also depend linearly on composition. The magnitude of the slope did not appear to correlate with band assignment or peak position. The greatest departures from nonlinearity occur for the closely spaced modes between 300 and 400 cm^{-1}, which are probably mixed modes. Mixed modes can behave oddly with com-

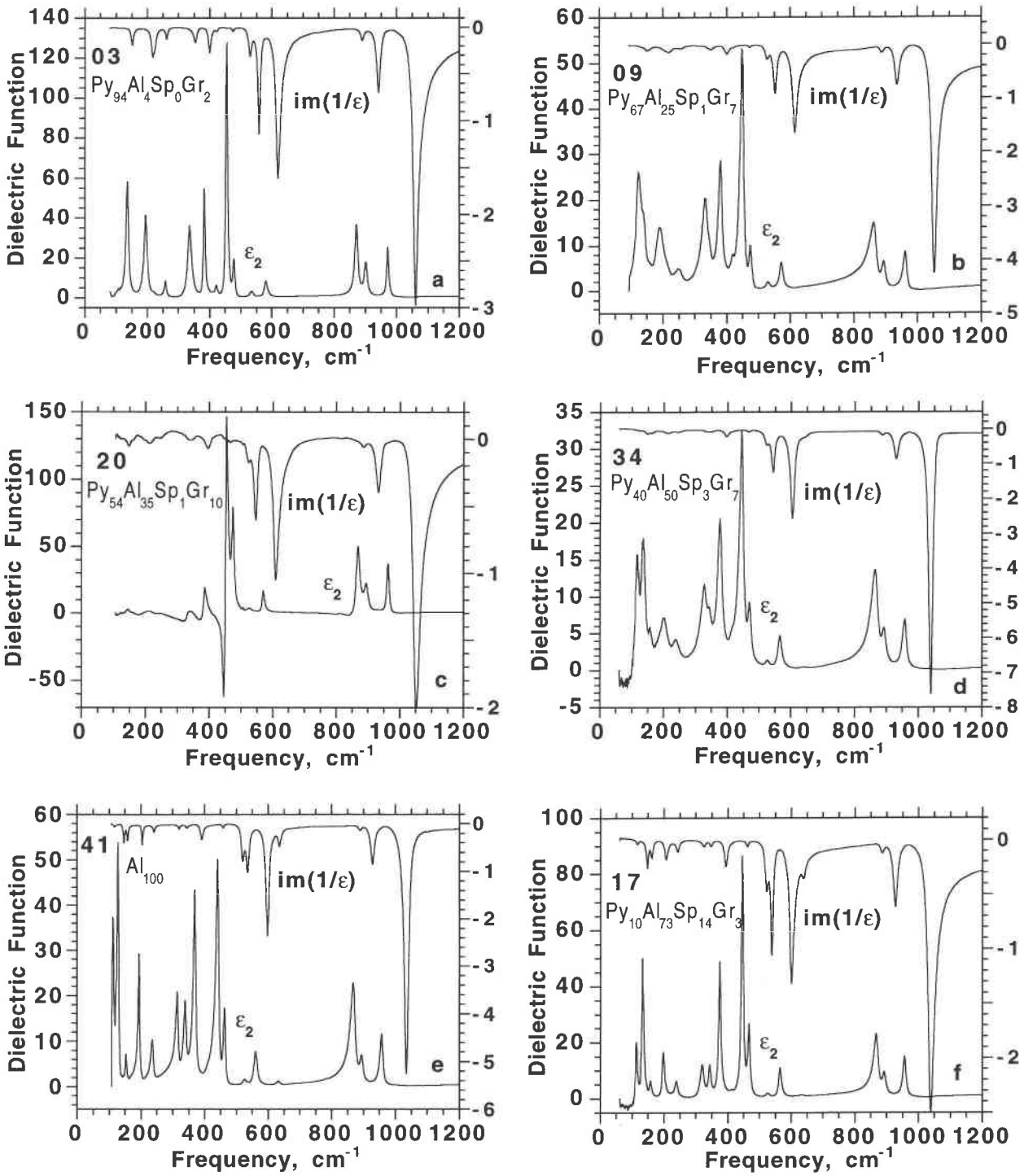

FIGURE 2. The dielectric functions ϵ_2 (lower lines) and imaginary parts im(1/ϵ) (upper lines) of samples 3, 9, 20, 34, 41, and 17 (a–f, respectively). Sample number and composition are shown on left. Sample numbers 7, 11, 18, 30, 33, 38, 40, and 43 have been deposited.

position if the degree of mixing changes across the binary. Variation in mixing is indicated here because pyrope has accidental degeneracies that almandine lacks. The sample most affected is 20, but because its peak positions are approximate, its slight departure from the trend may not be significant.

The two samples with high Mn content are very similar in appearance to the other samples with high almandine

TABLE 3. Infrared frequencies*

Index		3	18	9	7	40	43
Approx. comp.**		$Py_{95}Al_5$	$Py_{72}Al_{28}$	$Py_{67}Al_{33}$	$Py_{60}Al_{40}$	$Py_{58}Al_{42}$	$Py_{54}Al_{46}$
Gr + Uv + An		1.8	9.5	7.4	7.5	3.0	4.5
Mode	assign.†						
B	ν_3	972.0–1060.0	965.8–1056.3	961.8–1053.7	961.8–1009.2	962.7–1048.3	963.3–1049.7
C	ν_3	901.7–890.0	897.2–886.9	894.4–888.6	894.4–887.1	895.5–890.0	895.9–890.0
D	ν_3	871.0–941.3	867.8–935.6	862.2–935.4	863.6–934.0	867.4–935.4	866.6–935.4
	overtone	~750	813.8–815.1				
E	ν_4	~650	~648	~647	~647	647.7–649.1	647.0–653
F	ν_4	580.9–620.4	574.4–615.0	572.0–614.6	572.8–611.6	570.7–610.2	570.6–610.2
G	ν_4	535.4–557.4	530.6–553.3	531.0–553.0	529.6–550.1	529.2–548.6	529.6–548.6
	overtone			~500	~500	507.5–508.3	506.8
H	T_{oct}	478.3–475.4	476.7–467.2	475.4–472.4	473.9–471.1	470.6–469.2	471.0–468.9
I	ν_2	454.8–529.6	445.0–527.8	449.0–528.1	450.2–526.6	445.0–526.6	444.6–526.0
J	T_{oct}	421.7–423.0	417.2–419.4	419.7–420.0	419.1–420.9	416.9–418.2	416.7–417.3
K	R	383.0–399.9	380.6–398.3	381.6–400.8	381.0–399.7	377.8–397.7	377.2–397.5
L	R	336.2–357.3		345.7–351.3	344.8–350.8	341.2–349.9	341.0–349.1
M	T	336.2–357.3	328.3–349.4	333.2–341.6	333.2–342.0	329.0–339.3	328.8–339.2
	$T_{SiO_4,Gr}$						
O	T_{oct}	258.5–263.0	249.8–257.3	249.7–256.3	246.8–251.3	241.1–250.1	239.4–249.7
P_{Mg}	$T_{dod,\,Mg}$	220.8–223.0	215–213	~212	~210		
N	T_{dod}	194.6–218.1	191.5–218.8	191.0–217.8	189.6–217.4	194.7–215.7	194.0–215.6
	$T_{dod,\,Ca}$						
P_{Fe}	$T_{dod,\,Fe}$			158.4–162.9	157.4–166.8	156.8–163.0	157.4–161.8
Q	T_{dod}	134.4–152.2	142–138.7	136.9–150.1	136.9–150.2	137.3–149.0	135.4–149.1
R	T	134.4–152.2	125.9–151.5	122.2–135.4	120.8–134.4	122.6–131.5	117.8–129.4
	?(see text)	~105					

* Listed as TO-LO with each position in inverse centimeters. The uncertainty in the last digit is ±1.

** "Al" content is the sum of all components except pyrope. Spessartine content is separately enumerated if >10 mol%.

† Assignments are based on those for almandine by Hofmeister and Chopelas (1991), where ν_3 is the asymmetric stretching motion of the SiO_4 tetrahedron, ν_4 is the asymmetric bending motion of the SiO_4 tetrahedron, ν_2 is the symmetric bending motion of the SiO_4 tetrahedron, T_{oct} is a translation of the octahedrally coordinated cations against the O sublattice, R is a rotation-libration of the SiO_4 tetrahedron, T_{dod} indicates translations of the cations in the approximately dodecahedral interstice, and T indicates a translation of the tetrahedron.

‡ Several weak bands are present near this position.

§ Positions were estimated from the raw reflectivity.

content (Fig. 1, Table 3). The IR frequencies of garnet sample 17 with 15 mol% spessartine lie slightly below the trend defined by nearly pure pyrope-almandine samples, whereas the frequencies of sample 30 with 10 mol% spessartine lie on the trend (Fig. 3). The comparison indicates that it is reasonable to combine the contents of spessartine and almandine for minor amounts of Mn.

Sample 18 with high Ca content (10 mol% grossular + uvarovite + andradite) falls on the pyrope-almandine trend. Sample 20 with similarly high Ca content has high-frequency peaks that lie on the trends, but the low-frequency peaks may lie below. Because these low-frequency peak positions were estimated, their departures from the trends are probably due to the larger experimental uncertainties and hence may not be real. In addition, this sample has extra peaks at 292 and 178 cm^{-1}, which could have affected the frequencies of the neighboring bands. The interdependency of the IR peak positions is implicit in the mathematical description of the reflectivity (e.g., Wooten 1972) and can be readily seen in classical dispersion analyses (e.g. Spitzer et al. 1962). Also, most modes are not pure but have some degree of mode mixing.

The IR frequencies also depend linearly on pyrope + grossular + andradite + uvarovite content (Fig. 3b). Clearly, minor amounts of impurities have a negligible effect on the values of the frequencies; more than 10 mol% of an impurity (e.g., andradite, uvarovite, spessartine, or grossular components in the pyrope-almandine system) discernibly affects the peak positions; whereas impurity contents near 10 mol% have at most a minor effect.

DISCUSSION AND CONCLUSIONS

General

Linear trends of mid-IR frequencies with composition along the pyrope-almandine binary have been previously observed for spectra obtained from dispersed powders (Geiger et al. 1989). Our data corroborate these results and further show that the linear trends hold for all the lattice modes. The frequencies of overtones also depend linearly on composition.

The excellent agreement of the intensity patterns and peak positions of the synthetic almandine with the natural spessartine sample 30, and of the synthetic intermediate sample 43 with 54.7 mol% pyrope with the natural samples 40 and 20, indicates that quantitative measurements can be obtained from reflectance spectra of polycrystals. Obviously, this statement is true only for isotropic substances because structures with lower symmetry have polarization effects.

Two-mode behavior

For some solid solutions, IR peak positions vary smoothly with composition along the series (one-mode

TABLE 3.—*Continued*

20 $Py_{54}Al_{46}$ 9.9	33 $Py_{44}Al_{56}$ 6.4	34 $Py_{40}Al_{60}$ 7.1	11 $Py_{18}Al_{82}$ 3.6	17 $Py_{10}Al_{76}Sp_{14}$ 2.6	30 $Py_{8}Al_{82}Sp_{10}$ 2.2	38 $Py_{6}Al_{94}$ 5.9	41 Al_{100} 0.0
963.0–1052.1	958.9–1042.4	958.9–1039.5	960.3–1043.9	957.0–1039.4	956.3–1034.1	957.4–1036.5	957.4–1035.1
894.4–886.3	892.9–887.1	892.9–887.1	895.9–888.6	893.0–886.2	893.0–887.7	892.9–887.1	894.4–888.6
869.2–932.9	865.1–932.5	863.6–930.2	871.0–931.0	867.0–927.5	866.5–927.9	869.5–928.1	868.0–928.1
−815.4		~750	~700				~712
648–~652	645 2–645.5	641.5–643.4	637.2–639.5	635.2–638.6	635.4–637.6	633.6–637.2	633.2–636.5
570.5–610.3	566.2–605.8	566.2–604.3	569.1–604.3	565.0–601.1	562.5–599.2	561.8–598.4	561.4–598.4
526.9–546.2	526.2–545.7	526.6–542.8	528.1–541.3	526.6–539.0	526.1–537.6	525.2–537.3	526.2–535.4
506.5	506.6–506.5	505.8	508.7–~510		~500‡		
474.3–467	468.0–466	469.5–466.2	468.0–462.9	466.9–461.6	463.4–461.2	465.1–461.8	462.2–457.8
~445–525.0§	440.2–522.4	444.6–522.2	447.5–523.7	445.8–522.2	437.6–521.7	443.1–522.2	441.7–520.8
410–418§	415.8–418.0	416.7–418.9	414.5–415.7	413.7–415	~411	413.5–414.2	412–415
371–395.6§	369.9–396.4	377.2–396.9	375.7–394.7	375.3–394.2	370.0–393.9	374.3–394.4	369.9–390.5
~340–342.7§	339.9–348.8	342.1–348.0	343.1–346.9	343.8–347.7	340.7–347.1	342.7–347.6	339.1–343.5
313–340§	320.4–330.2	328.0–336.5	323.0–327.7	320.3–325.1	315.8–324.5	318.6–322.5	314.2–320.0
~292§							
232–246.2§	235.0–246.2	238.5–244.2	238.7–242.5	239.0–243.4	237.3–242.9	238.0–242.1	236.5–240.9
187–214.5§	197.0–214.5	200.4–212.9	198.4–206.3	198.7–206.9	195.7–206.2	195.5–204.0	194.0–204.0
~178§							
157–162.4§	157.4–163.8	157.9–162.3	156.0–161.2	158.0–161.9	156.1–161.4	156.7–160.0	153.0–157.4
133–147.9§	133.9–150.4	136.9–148.6	134.0–148.0	132.8–148.5	130.6–148.4	131.0–147.6	128.1–145.7
110–123§	117.8	117.8–123.9	116.4–118.9	113.8–117.7	112.8–118.1	112.0–115.3	112.0–117.8

behavior). For other solid solutions, bands appear that are characteristic of each end-member. These may vary in peak position, but the main change is in relative intensity with composition along the series (two-mode behavior). Two-mode behavior originates in local modes associated with impurity ions and is expected if substantial differences exist among the masses of substituting ions or among the force constants (Chang and Mitra 1968) and if end-member band profiles do not overlap (Fertel and Perry 1979). In structures with more than two atomic sites (e.g., perovskites), some IR bands may exhibit one-mode behavior, whereas other bands exhibit two-mode behavior (Barker et al. 1968). Two-mode behavior was reported for translations of the SiO_4 tetrahedron in solid solutions between grossular and pyrope (or almandine) garnet (Hofmeister and Chopelas 1991), for the stretching modes and translations of the tetrahedra in solid solutions of $Y_3Al_2Al_3O_{12}$ and $Mn_3Al_2Si_3O_{12}$ (Lu et al. 1993), and for translations of Al and Fe^{3+} cations in the octahedral site of grossular-andradites (McAloon and Hofmeister 1995).

For pyrope-almandine solid solutions, the large mass difference between Mg and Fe could cause two-mode behavior if the end-member peaks are well separated. The disappearances of one pair of modes at 221 cm^{-1} in pyrope and at 158 cm^{-1} in almandine as composition progresses is compatible with two-mode behavior. All other peaks follow one-mode behavior, owing to either small separations of the end-member peaks or the lack of participation of Mg or Fe in the vibration.

Band assignments

Assignment of the observed IR peaks to atomic motions (Table 3) is based on symmetry analysis (Moore et al. 1971), previous IR data on chemical substitutions among garnets (Hofmeister and Chopelas 1991), data from the $Mn_3Al_2Si_3O_{12}$-$Y_3Al_2Al_3O_{12}$ (YAG) binary (Lu et al. 1993), data from the grossular-andradite binary (McAloon and Hofmeister 1995), and data presented here. The trends observed in Figures 3a and 3b require that previous assignments (Hofmeister and Chopelas 1991) for the IR modes at 134 and 260 cm^{-1} in pyrope be revised (Table 3). The old assignments were made by pairing peaks of the end-members, which was difficult because two peaks are degenerate in pyrope. The assignment of IR peaks to atomic motions is a first approximation in which mode mixing is assumed to be negligible. We do not imply that the contributions of atomic motions from individual sites in garnet represent localized vibrations.

The two-mode behavior observed for the bands at 221 cm^{-1} in pyrope and at 158 cm^{-1} in almandine is consistent with assignment to translations of the dodecahedral cation (Table 3). Other motions predicted by symmetry analysis (Moore et al. 1971; Hofmeister and Chopelas 1991) lack the requisite large mass differences. Large differences in force constants are not indicated for the substitution of Mg for Fe^{2+} because the IR frequencies of pyrope and almandine differ only slightly. Symmetry analysis predicts that three translations involving the dodecahedral site should occur. The two other dodecahedral translations at 195 and 134 cm^{-1} in pyrope and at 199 and 133 cm^{-1} in almandine do not meet the criteria of nonoverlapping peaks.

The additional low-frequency bands in sample 20 are local modes assigned to a translation of the dodecahedron containing Ca and to a translation of the tetrahedron adjacent to Ca. The later vibration occurs as a local mode

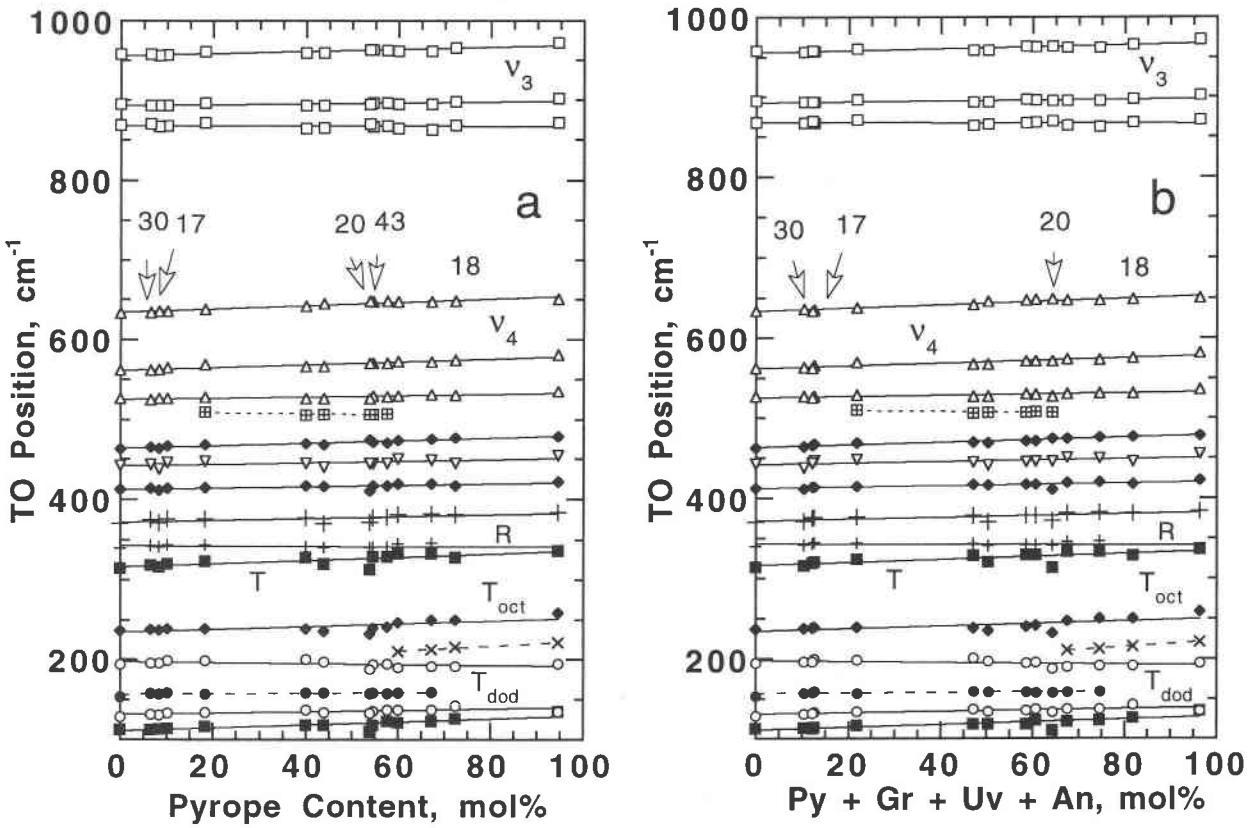

FIGURE 3. IR frequencies of pyrope-almandine fundamental TO modes as a function of composition. Uncertainties in frequency are smaller than the symbol. (**a**) Pyrope content was separated from all the other garnet components. (**b**) Pyrope content was grouped with that of the calcic garnet components. Symbols: open squares = ν_3, squares with crosses = overtone, triangles = ν_4, diamonds = T_{oct}, inverted triangles = ν_2, plus signs = R, solid squares = T, Xs = T(Mg), solid circles = T_{Fe}, open circles = T_{dod}. Least-squares fits are shown as solid lines for bands exhibiting one-mode behavior and as dashed lines for two-mode behavior. Dotted lines represent overtones. Small labels are sample numbers.

because it is mixed with T_{dod} as shown by the spessartine-YAG series (Lu et al. 1993).

Frequency, composition, and structure

Frequency depends on atomic mass, bond length, and the strength of the chemical bond. The molar volumes of mixing of pyrope-almandine garnets are ideal (e.g., Geiger et al. 1987). Hence, the approximately linear dependence of frequency on composition (Figs. 3a and 3b) is attributed to structural changes in the series because mass differences pertain to only three modes and are accounted for in the existence of two-mode behavior. The linear behavior of the frequencies further suggests that changes in the bond strength are mainly derived from variations of the bond length. If changes in bond strength occur simply as a result of the substitution of Mg for Fe^{2+}, then this contribution is also linearly dependent on composition for the series.

The fact that samples with up to 10 mol% grossular or spessartine lie on or near the trend for the pyrope-almandine series shows that impurities have a minor effect on the spectra. Our observations are compatible with the study of Koziol and Newton (1989), who showed that the volume of a garnet with a given $Mg/(Mg + Fe^{2+})$ ratio is proportional to the grossular content. Thus, as Ca content in garnets increases, the volume increases, and the frequencies of the modes associated with translations of the cations fall below the trend of the binary samples, as observed for Figure 3a. Given the slight influence of Ca in garnet with minor grossular contents, small amounts of Fe^{3+}, Ti, Cr, and the presence of OH should not significantly affect the lattice modes.

Mixing properties

The approximately linear dependence of the vibrational frequencies on composition along the pyrope-almandine join is pertinent to the compositional dependence of macroscopic properties. Bulk moduli calculated by applying Hofmeister's (1991) model to the vibrational data for this series are predicted to depend linearly on com-

TABLE 4. Linear representation of pyrope-almandine TO modes

Mode	Assign.	ν_0* (cm^{-1})	$d\nu/dX$ (cm^{-1}/mol% Py)	R**
B	ν_3	955.7	0.13	0.89
C	ν_3	893.5	0.056	0.96
D	ν_3	867.5	−0.012	0.12
E	ν_4	633.9	0.21	0.96
F	ν_4	561.5	0.18	0.93
G	ν_4	525.0	0.080	0.85
	overtone	509.9	−0.060	0.14
H	T_{oct}	463.4	0.16	0.95
I	ν_2	441.2	0.10	0.63
J	T_{oct}	411.9	0.09	0.76
K	R	371.2	0.11	0.72
L	R	342.2	−0.017	0.19
M	T	316.1	0.20	0.77
O	T_{oct}	234.1	0.18	0.70
N	T_{dod}	196.9	−0.059	0.46
P_{Mg}	$T_{dod, Mg}$	191.5	0.31	0.98
P_{Fe}	$T_{dod, Fe}$	156.6	0.035	0.6
Q	T_{dod}	130.9	0.09	0.72
R	T	110.5	0.19	0.82

* The initial frequencies are those of almandine.
** R is the multiple-correlation coefficient. See Bevington (1969) for discussion.

position along the pyrope-almandine join, in agreement with previous observations (e.g., Babuska et al. 1978). Similarly, the lattice contribution to the thermodynamic properties such as heat capacity and entropy follows ideal mixing laws because these quantities are integrals of various functions involving the vibrational frequencies (Kieffer 1979). This inference contrasts with conclusions of previous workers (e.g., Ganguly and Saxena 1984; Berman 1990) that pyrope-almandine garnets behave as ionic solutions but are not ideal. The discrepancy could arise from magnetic and electronic interactions behaving nonlinearly with composition in that the system changes from having isolated Fe^{2+} ions to juxtaposed and probably interacting Fe^{2+} ions. This hypothesis could be tested by calculating the magnetic and electronic contributions to heat capacity and entropy from optical spectroscopic measurements (e.g., Burns 1985).

The small deviations of frequency from the linear trends (Fig. 3) for samples with low Ca content (<10 mol% grossular + andradite + uvarovite) is compatible with the previous work: Koziol and Newton (1989) concluded that volumes of mixing are nearly ideal for samples with low Ca content (<30 mol%).

ACKNOWLEDGMENTS

We heartily thank F. Barker (U.S. Geological Survey), R.M. Hazen (Geophysical Laboratory), A. Koziol (University of Dayton), W. Metropolis (Harvard University), and J.R. Smyth (University of Colorado) for providing samples. We also thank S. Roeske (University of California, Davis) for help in obtaining microprobe data. Many thanks also to N. Winter (University of California, Davis) for help in sample preparation and to K. Viskupic (Washington University) for preparing the figures. Support was provided by the David and Lucile Packard Foundation and by NSF grant EAR-9496266.

REFERENCES CITED

Aines, R.D., and Rossman, G.R. (1984a) The water content of mantle garnets. Geology, 12, 720–723.
——— (1984b) The hydrous component in garnets: Pyralspites. American Mineralogist, 69, 1116–1126.
Andermann, G., Caron, A., and Dows, D.A. (1965) Kramers-Kronig dispersion analysis of infrared reflectance bands. Journal of the Optical Society of America, 55, 1210–1216.
Babuska, V., Fiala, J., Kumazawa, M., Ohno, I., and Sumino, Y. (1978) Elastic properties of garnet solid-solution series. Physics of the Earth and Planetary Interiors, 16, 157–176.
Barker, A.S., Jr., Ditzenberger, J.A., and Guggenheim, H.J. (1968) Long-wavelength optical lattice vibrations in mixed $KMgF_3$-$KNiF_3$ crystals. Physical Review, 175, 1180–1190.
Barker, F. (1964) Reaction between mafic magmas and pelitic schist, Cortlandt, New York. American Journal of Science, 262, 614–634.
Bell, D.R., Ihinger, P.D., and Rossman, G.R. (1995) Quantitative analysis of trace OH in garnet and pyroxenes. American Mineralogist, 80, 465–474.
Berman, R.G. (1990) Mixing properties of Ca-Mg-Fe-Mn garnets. American Mineralogist, 75, 328–344.
Bevington, P.R. (1969) Data reduction and error analysis for the physical sciences, 36 p. McGraw-Hill, New York.
Burns, R.G. (1985) Thermodynamic data from crystal field spectra. In Mineralogical Society of America Reviews in Mineralogy, 14, 277–316.
Chang, I.F., and Mitra, S.S. (1968) Application of a modified long-range iso-displacement model to long-wavelength optic phonons of mixed crystals. Physical Review, 172, 924–933.
Chopin, C. (1984) Coesite and pure pyrope in high-grade blueschists of the Western Alps: A first record and some consequences. Contributions to Mineralogy and Petrology, 86, 107–118.
Deer, W.A., Howie, R.A., and Zussman, J. (1982) Rock-forming minerals, vol. 1A: Orthosilicates, 919 p. Longman, London, U.K.
Dowty, E. (1971) Crystal chemistry of titanian and zirconian garnet: I. Review and spectral studies. American Mineralogist, 56, 1983–2009.
Fertel, J.H., and Perry, C.H. (1979) Optical phonons in $KCl_{1-x}Br_x$ and $K_{1-x}Rb_xI$ mixed crystals. Physical Review, 184, 874–884.
Ganguly, J., and Saxena, S.K. (1984) Mixing properties of aluminosilicate garnets: Constraints from natural and experimental data, and applications to geothermo-barometry. American Mineralogist, 69, 88–97.
Geiger, C.A., Newton, R.C., and Kleppa, O.J. (1987) Enthalpy of mixing of synthetic almandine-grossular and almandine-pyrope garnets from high temperature solution calorimetry. Geochimica et Cosmochimica Acta, 51, 1755–1763.
Geiger, C.A., Winkler, B., and Langer, K. (1989) Infrared spectra of synthetic almandine-grossular and almandine-pyrope garnet solid-solutions: Evidence for equivalent site behavior. Mineralogical Magazine, 53, 231–238.
Hietanen, A. (1963) Metamorphism of the Belt series in the Elk River-Clarkia area, Idaho. U.S. Geological Survey Professional Paper 344-C, 78 p.
Hofmeister, A.M. (1991) Calculation of bulk moduli and their pressure derivatives from vibrational frequencies and mode Grüneisen parameters: Solids with cubic symmetry or one-nearest-neighbor distance. Journal of Geophysical Research, 96, 16181–16203.
——— (1995) Infrared microspectroscopy in the earth sciences. In H. Humicki, Ed., Practical guide to infrared microspectroscopy, p. 377–416. Marcel Dekker, New York.
Hofmeister, A.M., and Chopelas, A. (1991) Vibrational spectroscopy of end-member silicate garnets. Physics and Chemistry of Minerals, 17, 503–526.
Hofmeister, A.M., and Campbell K.R. (1992) Infrared spectroscopy of yttrium iron, yttrium gallium, and yttrium aluminum garnets. Journal of Applied Physics, 72, 638–646.
Huggins, F.E., Virgo, D., and Huckenholz, H.G. (1977a) Titanium-containing silicate garnets: I. The distribution of Al, Fe^{3+}, and Ti^{4+} between octahedral and tetrahedral sites. American Mineralogist, 62, 475–490.
——— (1977b) Titanium-containing silicate garnets: II. The crystal chem-

istry of melanites and schorlomites. American Mineralogist, 62, 646–665.

Kieffer, S.W. (1979) Thermodynamics and lattice vibrations of minerals: 3. Lattice dynamics and an approximation for minerals with application to simple substances and framework silicates. Reviews in Geophysics and Space Physics, 17, 35–39.

Koziol, A., and Newton, R.C. (1989) Grossular activity-composition relationships in ternary garnets determined by reversed displacement-equilibrium experiments. Contributions to Mineralogy and Petrology, 103, 423–437.

Lu, R., Jackson, K.D., and Hofmeister, A.M. (1993) Thin-film infrared spectra from solid solutions of spessartine and yttrium aluminum garnet. Canadian Mineralogist, 31, 381–390.

MacGregor, I.D., and Manton, W.I. (1986) Roberts Victor eclogites: Ancient oceanic crust. Journal of Geophysical Research, 91, 14063–14079.

McAloon, B.P., and Hofmeister, A.M. (1993) Single-crystal absorption and reflection infrared spectroscopy of birefringent grossular-andradite garnets. American Mineralogist, 78, 957–967.

——— (1995) Single-crystal IR spectroscopy of grossular-andradite garnets. American Mineralogist, 80, 1145–1156.

Moore, R.K., White, W.B., and Long, T.V. (1971) Vibrational spectra of the common silicates: I. The garnets. American Mineralogist, 56, 54–71.

Novak, G.A., and Gibbs, G.V. (1971) The crystal chemistry of the silicate garnets. American Mineralogist, 56, 791–825.

Pabst, A. (1943) Large and small garnets from Fort Wrangell, Alaska. American Mineralogist, 28, 233–245.

Rossman, G.R., Beran, A., and Langer, K. (1989) The hydrous component of pyrope from the Dora Maira Massif, Western Alps. European Journal of Mineralogy, 1, 151–154.

Schaal, R.B. (1991) I. Geometric modeling in reaction space of mineralogical diversity among eclogites, II. Constraints on shallow subduction of the Farallon plate from mantle xenoliths of the Colorado Plateau, 128 p. Ph.D. dissertation, University of California, Davis.

Schwartz, K.B., Nolet, D.A., and Burns, R.G. (1980) Mössbauer spectroscopy and crystal chemistry of natural Fe-Ti garnets. American Mineralogist, 65, 142–153.

Spitzer, W.G., Miller, R.C., Kleinman, D.A., and Howarth, L.E. (1962) Far-infrared dielectric dispersion in $BaTiO_3$, $SrTiO_3$, and TiO_2. Physical Review, 126, 1710–1721.

Tarte, P. (1965) Etude experimentale et interpretation du spectre infrarouge des silicates et germanates: Application á des problemes structurauz relatifs a le état solide. Memoires de l'Academie Royale de Belgique, 35(4a), 1–259; 35(4b), 1–134.

Thompson, P.J. (1985) Stratigraphy, structure and metamorphism in the Moradnock quadrangle, New Hampshire, 191 p. Contribution no. 58, Department of Geology and Geography, University of Massachusetts, Amherst.

Wooten, F. (1972) Optical properties of solids, 260 p. Academic, San Diego, California.

Manuscript received June 8, 1995
Manuscript accepted November 13, 1995